

# Color Restoration for Infrared Cutoff Filter Removed RGBN Multispectral Filter Array Image Sensor

Chul Hee Park, Hyun Mook Oh and Moon Gi Kang

*Institute of BioMed-IT, Energy-IT and Smart-IT, Technology (BEST), Yonsei University,  
50 Yonsei-Ro, Seodaemun-Gu, Seoul, South Korea*

**Keywords:** Multi Spectral Image, Color Restoration, Spectral Estimation, Low Light Condition, Spectral Decomposition, Multi Filter Array, Infrared Cut Off Filter Removal.

**Abstract:** Imaging systems based on multispectral filter arrays (MSFA) can simultaneously acquire wide spectral information. A MSFA image sensor with R, G, B, and near-infrared (NIR) filters can obtain the mixed spectral information of visible bands and that of the NIR bands. Since the color filter materials used in MSFA sensors were almost transparent in the NIR range, the observed colors of multispectral images were degraded by the additional NIR spectral band information. To overcome this color degradation, a new signal processing approach is needed to separate the spectral information of visible bands from the mixed spectral information. In this paper, a color restoration method for imaging systems based on MSFA sensors is proposed. The proposed method restores the received image by removing NIR band spectral information from the mixed wide spectral information. To remove additional spectral information of the NIR band, spectral estimation and spectral decomposition were performed based on the spectral characteristics of the MSFA sensor. The experimental results show that the proposed method restored color information by removing unwanted NIR contributions to the RGB color channels.

## 1 INTRODUCTION

In most digital cameras, CCD or CMOS image sensors are used to acquire the light reflected by objects. Unlike human eyes, sensors based on silicon ( $\text{SiO}_2$ ) are sensitive to near-infrared (NIR) up to 1100nm, limited by the cut-off of silicon. To prevent unnatural looking images, digital cameras are usually equipped with infrared cut-off (IRCF) filter. This filter, sometimes called IR filter or hot mirror, reflect or block near infrared wavelengths from about 700nm to 1100nm while allowing visible light to enter.

However, because of this characteristic of IRCF, image sensors cannot receive much valuable information outside of the visible spectrum. For instance, most dyes and pigments used for material colorization are somewhat transparent to NIR. Therefore, the difference in the NIR intensities is not only due to the particular color of the material, but also the absorption and reflectance characteristics of the dyes. Therefore, the NIR intensity gives the information pertinent to material classes rather than the color of that object (Salamati and Susstrunk, 2010).

Recently, there have been several attempts to use NIR band information. In remote sensing applications

(J. Choi and Kim, 2011), the multi-spectral images observed in a variety of the spectrum bands are used where both visible and NIR bands are included. As each spectral band provides different information, the spectral bands are selectively used in the observation of the multi-spectral images.

In surveillance cameras (X. Hao and Wang, 2010), the NIR band is used especially in low light conditions or invisible NIR light conditions. The NIR band is also used in biometric (Kumar and Prathyusha, 2009), face matching (D. Yi and Li, 2007), and face recognition (S. Z. Li and Lun, 2007) applications, which have been studied based on the intrinsic reflectivity of the skin or eyes under NIR illumination. Since the reflection in NIR is material dependent, it is also used in material classification (Salamati and Susstrunk, 2010) and illuminant estimation (Fredembach and Susstrunk, 2009). NIR images can be used in image enhancement applications such like image dehazing (L. Schaul and Susstrunk, 2009).

Kise et al. designed a three-band spectral imaging system composed of multiple cameras with a beam splitter (M. Kise and Windham, 2010). This imaging system has been used to acquire multispectral images in user-selected spectral bands simultaneously by uti-

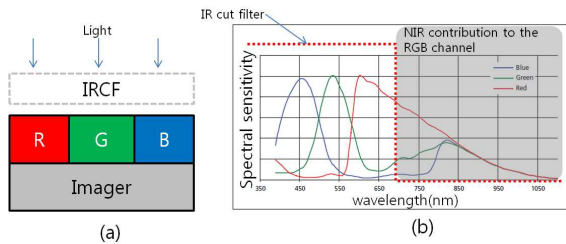


Figure 1: (a) Conventional camera system based on CFA image sensor with IR-cut filter. (b) Spectral sensitivity of the camera system.

lizing three interchangeable optical filters and various optical components. Similarly, Matsui et al. implemented a multispectral imaging system, where two IRCF removed cameras were used to capture the color and NIR images, independently (S. Matsui and Sato, 2010). In this system, the IRCF removed cameras are perpendicularly aligned and the IRCF was used as a light splitter for visible and NIR bands. By managing the shutter of two cameras with a single controller, each spectral band image pair was acquired, simultaneously. However, this imaging system requires a large place to fix two or more cameras and an alignment process. Due to the lack of portability of the devices, multi-camera based imaging systems are not suitable for outdoor environments.

As an alternative approach, an IRCF removed color filter array (CFA) image sensor like a Bayer image sensor without an IRCF can be used (Fredembach and Susstrunk, 2008). By using a single digital camera without IRCF, the spectral information of the visible band and that of the NIR band can be acquired at the same time. Fig. 1 shows a conventional camera system approach with an IRCF and a spectral sensitivity of a MOS imager integrated with traditional organic on-chip RGB Bayer filters. By removing the IRCF, the NIR contribution to the RGB channel reaches the MOS imager.

On the other hand, mixing color and NIR signals on the pixel level can result in extreme color desaturation if the illumination contains high amounts of NIR. Although it may be possible to overcome the unwanted NIR contribution to the RGB color channel through the signal processing technique, it is hard to estimate the NIR spectral energy in each RGB color channel because there is no way to detect the NIR band spectral characteristics.

As an improved system based on the single image sensor, an imaging system based on a multispectral filter array (MSFA) which simultaneously obtains visible and NIR band images can be considered (S. Koyama and Murata, 2008). A pixel configuration of the RGB filters and another NIR pass filter, which transmits NIR light only, is shown in Fig.2. With the

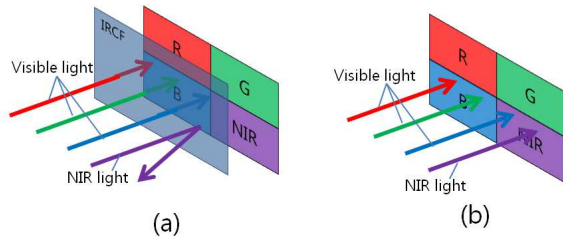


Figure 2: The Infrared cut off filter. (a) Typical imaging system using IRCF. (b) IRCF removed imaging system.

use of this filter configuration, RGB signals can be calculated by subtracting a NIR signal from RGB signals that have deteriorated with the NIR components. As a result, the IRCF can be removed even during the day. Because of this advantage, imaging systems based on MSFA sensors can be applied to a wide variety of applications. Furthermore, if fusion technology that uses NIR band information is applied, it is possible to gain additional sensitivity to color which does not deviate significantly from the human visual system.

This paper proposes a color restoration method that removes the NIR component in each RGB color channel with an imaging system based on the IRCF removed MSFA image sensor. Since the color degradation caused by the IRCF removal is a huge limitation, the NIR contribution to each RGB color channel needs to be eliminated. To remove unwanted NIR components in each RGB channel, the color restoration model is subdivided into two parts : spectral estimation and spectral decomposition.

## 2 PROBLEM STATEMENT

### 2.1 Color Model of an IRCF removed MSFA Image Sensor

The color image observed by an IRCF removed MSFA image sensor can be modeled as a spectral combination of three major components: illuminant spectra  $E(\lambda)$ , sensor function  $R^{(k)}(\lambda)$ , and surface spectra  $S(\lambda)$ . The color image formation model for channel  $k$ ,  $C^{(k)}$ , is defined as (K. Barnard and Funt, 2002):

$$\begin{aligned}
 C^{(k)} &= \int_{w_{expand}} E(\lambda)R^{(k)}(\lambda)S(\lambda)d\lambda \quad (1) \\
 &= \int_{w_{vis}} E(\lambda)R^{(k)}(\lambda)S(\lambda)d\lambda \\
 &\quad + \int_{w_{nir}} E(\lambda)R^{(k)}(\lambda)S(\lambda)d\lambda \\
 &= C_{vis}^{(k)} + C_{nir}^{(k)},
 \end{aligned}$$

where  $w_{expand}$ ,  $w_{vis}$  and  $w_{nir}$  represent the spectral range of the IRCF removed MSFA image sensor, the visible band between 400nm to 650nm, and the NIR band up to 650nm, respectively. Since the IRCF removed MSFA image sensor acquires the additional NIR band spectral energy up to 650nm wavelength, the range of these three major components should be expanded to the NIR band.  $C_{vis}^{(k)}$ ,  $C_{nir}^{(k)}$  represents the camera response for channel  $k$  by using the IRCF removed MSFA image sensor in the visible band, and the NIR band, respectively. For image sensors with RGBN filters, the intensities at each pixel position can be represented as,

$$\begin{aligned} R(i, j) &= R_{vis}(i, j) + R_{nir}(i, j) \\ G(i, j) &= G_{vis}(i, j) + G_{nir}(i, j) \\ B(i, j) &= B_{vis}(i, j) + B_{nir}(i, j) \\ N(i, j) &= N_{vis}(i, j) + N_{nir}(i, j). \end{aligned} \quad (2)$$

In Eq. (2), each pixel contains additional NIR band information. Since this information help to gain the sensitivity of the sensor, this feature can be useful under low light conditions. However, mixing color and NIR intensities can result in color degradation if the illumination contains high amounts of NIR.

## 2.2 Color Degradation

To correct the de-saturated color from the images acquired by MSFA image sensors, several conventional methods can be considered as described in (K. Barnard and Funt, 2002). Given the observed color vector  $\mathbf{Y}$  and the visible band color vector with canonical illuminance  $\mathbf{X}$ , the color correction obtained by a color constancy method can be represented in matrix form:

$$\mathbf{X} = \Phi^T \mathbf{Y} \quad (3)$$

where  $\Phi$  is a diagonal matrix whose component corresponds to the ratio between the canonical and the current illuminance of each channel. The illuminant color estimation was performed under unknown lighting conditions where pre-knowledge based approaches, such as gamut mapping (G. D. Finlayson, 2000) or the color correlation framework (G. D. Finlayson and Hubel, 2001) were used. However, the conventional color constancy method which does not consider the NIR contribution to the RGB channels is limited when it comes to restoring natural color. As a result, the color degradation caused by additive NIR band intensity cannot be corrected by the conventional color constancy method. Although each color is obtained under the same illuminant conditions

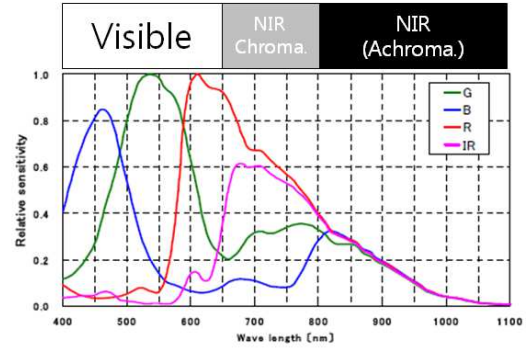


Figure 3: The spectral response of the MSFA image sensor.

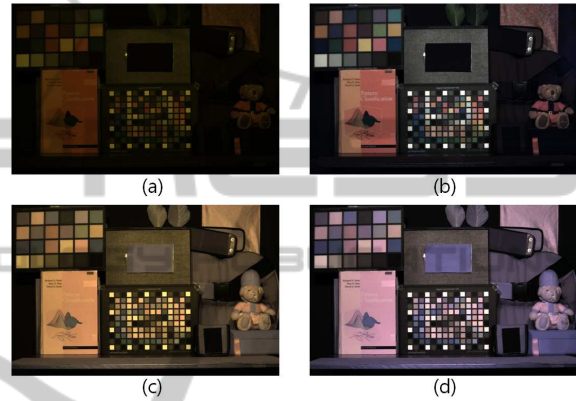


Figure 4: The color observation of the MSFA image sensor under incandescent light. (a) Image captured with IRCF. (b) (a) with color constancy. (c) Image captured with IRCF removal MSFA image sensor. (d) (c) with color constancy.

with and without an IRCF, respectively, the mixture of the exclusive NIR band intensity to the visible band intensity results in severe color distortion which alters the original color observation in the visible band.

Figure 4 describes the effect of the NIR band intensity in the color image. When objects were illuminated by an incandescent lamp, the image sensor with IRCF obtained a yellowish image due to the low color temperature of the illuminance. After performing the white balance technique from a grey color patch, a natural color image was obtained as shown in Fig. 4(b). On the other hand, when the IRCF was removed, the entire band of the image sensor was utilized and a broad spectral band image was observed. Due to additive NIR intensity in the RGB channels, Fig. 4(c) appears more brighter than Fig. 4(a) but shows low color saturation despite applying white balance in Fig. 4(d).

To analyze the change of the chromaticity feature obtained by the additional NIR, the RGB color space was converted into a HSI color space as follows,

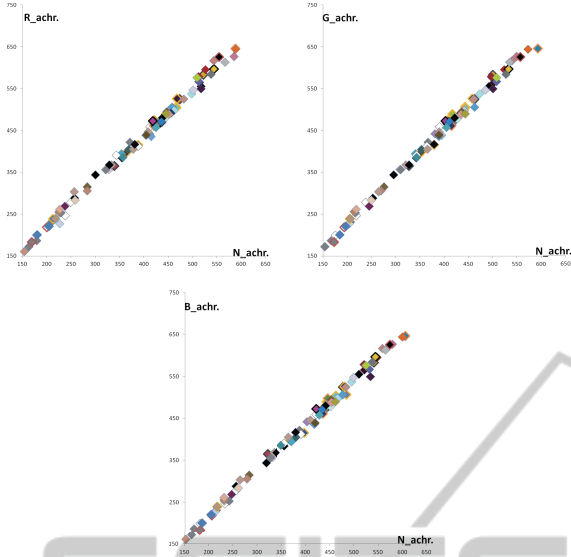


Figure 5: RGBN channel correlation in the NIR band above 800nm. (a)  $N_{nir}$  vs  $R_{nir}$ . (b)  $N_{nir}$  vs  $G_{nir}$ . (c)  $N_{nir}$  vs  $B_{nir}$ .

$$H = \cos^{-1} \left\{ \frac{\frac{1}{2}[(R-G) + (R-B)]}{[(R-G)^2 + (R-B)(G-B)]^{1/2}} \right\} \quad (4)$$

$$S = \frac{I-a}{I} \quad \text{where } a = \min[(R, G, B)],$$

$$I = \frac{R+G+B}{3},$$

where  $\min(\cdot)$  represents the minimum value among the three values. In Fig. 3, the NIR band is divided into two sub bands: we defined these sub bands as a chromatic NIR band (650nm – 800nm) and an achromatic NIR band (800nm – 1100nm), respectively. Figure 5 shows that the responses of the achromatic NIR bands were identical to each other. Based on this characteristic of the CMOS sensor in the NIR achromatic band, we defined these responses as constant at each pixel, such as  $R_{nir(achr)} = G_{nir(achr)} = B_{nir(achr)} = \delta$ . As a result, the RGB intensities at a pixel position in Eq. (2) were represented as:

$$\begin{aligned} R(i, j) &= R_{chr}(i, j) + \delta(i, j) \\ G(i, j) &= G_{chr}(i, j) + \delta(i, j) \\ B(i, j) &= B_{chr}(i, j) + \delta(i, j) \end{aligned} \quad (5)$$

where  $R_{chr}, G_{chr}, B_{chr}$  represent the chromatic colors of the image sensor under 800nm wavelength. With the RGB color values with offset  $\delta$ , the intensity of the observed color was defined as follows:

$$\begin{aligned} I &= \frac{[(R_{chr} + \delta) + (G_{chr} + \delta) + (B_{chr} + \delta)]}{3} \quad (6) \\ &= I_{chr} + \delta, \end{aligned}$$

where  $I_{chr} = (R_{chr} + G_{chr} + B_{chr})/3$  is the intensity of the chromatic spectral band of the image sensor. The

intensity of the IRCF removed MSFA image sensor is changed by the amount of the offset value. The hue value in Eq. (4) was redefined as:

$$\begin{aligned} H &= \cos^{-1} \left\{ \frac{\frac{1}{2}[(R-G) + (R-B)]}{[(R-G)^2 + (R-B)(G-B)]^{1/2}} \right\}, \quad (7) \\ &= \cos^{-1} \left\{ \frac{\frac{1}{2}[(R_{chr} - G_{chr}) + (R_{chr} - B_{chr})]}{[(R_{chr} - G_{chr})^2 + (R_{chr} - B_{chr})(G_{chr} - B_{chr})]^{1/2}} \right\}. \end{aligned}$$

Because the achromatic offset value  $\delta$  was removed during subtraction, the identical offset on the RGB channels did not change the hue value. Finally, the saturation value became:

$$S = \frac{I-a}{I} = \frac{I_{chr} - a_{chr}}{I} = \frac{I_{chr}}{I} \cdot S_{chr},$$

where  $S_{chr} = (I_{chr} - a_{chr})/I_{chr}$  represents the saturation of the chromatic spectral band of the image sensor and  $a_{chr} = \min(R_{chr}, G_{chr}, B_{chr})$ . Since the range of  $\frac{I_{chr}}{I}$  was  $0 \leq \frac{I_{chr}}{I} \leq 1$ , the saturation of the image obtained by the IRCF removed MSFA image sensor was degraded and became smaller than the image obtained by the chromatic spectral band of the image sensor.

### 3 PROPOSED METHODS

The purpose of the proposed method is to restore the original color in the visible band from the mixed wide band signal. However, color restoration in the spectral domain is an under-determined problem, as described in Eq. (2). Since MSFA image sensors have additional pixels whose intensity was represented in Eq. (2), this under-determined problem can be redefined with eight unknown spectral values. From Eq.(1), the observed intensity vectors of the multi-spectral images can be represented as  $C(i, j) = [R(i, j), G(i, j), B(i, j), N(i, j)]^T$ . To focus on the color restoration at each pixel position, we assumed the spatially sub-sampled MSFA image was already interpolated. As a result, there were four different intensities at each RGBN pixel position.

In Fig. 3, the spectral response of each channel is described with the corresponding RGB and N values. The energy of the NIR band was obtained by the RGB color filters as well as the N filter. Similarly, the large amount of the energy in the visible band was obtained by the N channel. By considering the observed multi-spectral intensity vector  $C(i, j)$ , the spectral correlation between the channels in the visible band and the NIR band resulted in a mixture of exclusive responses in each channel as represented in Eq. (2).

From the sub-spectral band intensity mixture model, the color restoration problem was defined to find the unknown visible band intensity values  $R_{vis}, G_{vis}, B_{vis}$  from the observed intensity values  $R, G,$

B, N which contained the unknown NIR band intensity values and the unknown visible intensity values.

### 3.1 Sensor Spectral Response Function Modeling

To restore the RGB channels corrupted by NIR band spectral energy, the additional NIR band components ( $R_{nir}$ ,  $G_{nir}$ ,  $B_{nir}$ ) in the RGB channels had to be removed:

$$\begin{aligned} R_{vis} &= R - R_{nir} \\ G_{vis} &= G - G_{nir} \\ B_{vis} &= B - B_{nir} \\ N_{vis} &= N - N_{nir} \end{aligned} \quad (8)$$

Since the spectral response function of the RGBN filter was not defined only in the NIR band, we used a signal processing approach to estimate the NIR band response. To decompose the spectral information of the RGBN channel, the unknown value  $N_{vis}$  or  $N_{nir}$  had to be estimated. To cope with the different characteristics of the correlation in the visible band as well as the NIR band, we set the correlation model in each subband, separately. In the visible band, the RGB channel filters showed different peak spectral responses while the N channel filter covered all spectral ranges without an outstanding peak. As a result, the N channel filter response function was modeled as a linear combination of the others:

$$\begin{aligned} N_{vis} &= \int_{400}^{700} \omega_r(\lambda) E(\lambda) R^{(r)}(\lambda) S(\lambda) d\lambda \\ &+ \int_{400}^{700} \omega_g(\lambda) E(\lambda) R^{(g)}(\lambda) S(\lambda) d\lambda \\ &+ \int_{400}^{700} \omega_b(\lambda) E(\lambda) R^{(b)}(\lambda) S(\lambda) d\lambda \end{aligned} \quad (9)$$

where  $\omega_r(\lambda)$ ,  $\omega_g(\lambda)$ , and  $\omega_b(\lambda)$  represent the coefficients that show cross-correlations in the visible band. Since the spectral response of the N channel in the visible band covered a wide spectral range without an outstanding peak, those coefficients were constrained to be constant in terms of the wavelength (Park and Kang, 2004). Using the constrained weights, the intensities of the N channel in the visible band were approximated as follows:

$$\begin{aligned} N_{vis}(i,j) &\approx \omega_r \cdot R_{vis}(i,j) \\ &+ \omega_g \cdot G_{vis}(i,j) + \omega_b \cdot B_{vis}(i,j), \end{aligned} \quad (10)$$

where  $\omega_r$ ,  $\omega_g$ , and  $\omega_b$  represent the visible band cross-correlation coefficients obtained by the linear transformation model:  $\mathbf{x}' = \mathbf{M}\mathbf{x}$ , where  $\mathbf{M}$  represents a 1 by 3 matrix describing the mapping between the RGB

to N channel values. The transformation  $\mathbf{M}$  was obtained by a least square solution. The weight function was of any arbitrary form caused by the illuminance change and the spectral response of the sensor. As a result, the function  $\omega$  depended not on the spectrum  $\lambda$  itself but on the spectral response of the illuminance and the sensor.

In the NIR band where the spectral correlations between the RGBN filters were high, there were numbers of coefficient sets in the application of the spectral decimation model. For instance, consider an extreme case of a single weight for one channel and zeros for the others or evenly distributed weights. Among a variety of solutions, we used visible band weights where the selection was a key to the relation between the exclusive two spectral bands. To cope with the different energy ratio in the visible and the NIR bands, the response of the N channel in the NIR band was:

$$\begin{aligned} N_{nir}(i,j) &\approx \beta_{v,n} \cdot (\omega_r \cdot R_{nir}(i,j) \\ &+ \omega_g \cdot G_{nir}(i,j) + \omega_b \cdot B_{nir}(i,j)) \end{aligned} \quad (11)$$

where  $\beta_{v,n}$  is the inter-spectral correlation coefficient that considers the energy balance between the visible band and the NIR band. When we decomposed the spectrally decomposed N channel in the visible and NIR bands, the given N channel was represented by the RGB channel intensities in the visible and NIR bands from Eq. (10) and Eq. (11).

$$\begin{aligned} N &= N_{vis} + N_{nir} \\ &= \omega_r \cdot (R_{vis} + \beta_{v,n} \cdot R_{nir}) + \omega_g \cdot (G_{vis} \\ &+ \beta_{v,n} \cdot G_{nir}) + \omega_b \cdot (B_{vis} + \beta_{v,n} \cdot B_{nir}) \end{aligned} \quad (12)$$

In Eq. (12), the observed N channel is described with unknown RGB values in the visible band and the NIR band. Therefore, we obtained the decomposed N channel indirectly from Eq. (12). Corresponding to the spectral response of the N channel, we defined the artificial N channel which was made by using the observed RGB channels and the inter-channel coefficients in Eq. (10).

$$\begin{aligned} \hat{N} &= \omega_r \cdot R + \omega_g \cdot G + \omega_b \cdot B \\ &= \omega_r \cdot (R_{vis} + R_{nir}) + \omega_g \cdot (G_{vis} + G_{nir}) \\ &+ \omega_b \cdot (B_{vis} + B_{nir}) \end{aligned} \quad (13)$$

Since the coefficients were designed to fit the N channel in the visible band, the estimated luminance resembled the N channel model in the visible band but not in the NIR band. Therefore, the N channel was decomposed into the visible and NIR bands by subtracting the original N channel in Eq. (12) and the artificial N channels  $\hat{N}$  in Eq. (13):

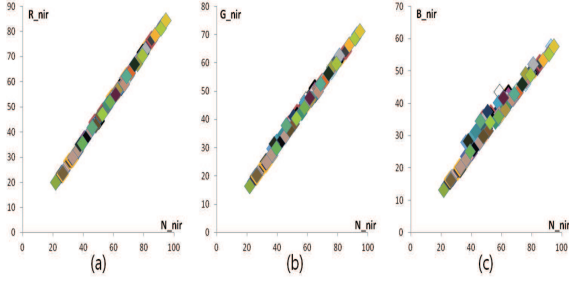


Figure 6: RGBN channel correlation in the NIR band. (a)  $N_{nir}$  vs  $R_{nir}$ . (b)  $N_{nir}$  vs  $G_{nir}$ . (c)  $N_{nir}$  vs  $B_{nir}$ .

$$\begin{aligned}
 N - \hat{N} &= \omega_r \cdot (\beta_{v,n} - 1) \cdot R + \omega_g \cdot (\beta_{v,n} - 1) \cdot G \\
 &\quad + \omega_b \cdot (\beta_{v,n} - 1) \cdot B \\
 &= (\beta_{v,n} - 1) \cdot (\omega_r \cdot R_{nir} + \omega_g \cdot G_{nir} + \omega_b \cdot B_{nir}) \\
 &= \frac{\beta_{v,n} - 1}{\beta_{v,n}} \cdot \hat{N}_{nir} \\
 &= \mathbf{K} \cdot \hat{N}_{nir}
 \end{aligned} \quad (14)$$

where  $K = \frac{\beta_{v,n} - 1}{\beta_{v,n}}$  is a scaling factor, and  $\hat{N}_{nir}$  represents the artificial N channel of NIR band from Eq. (11). Based on Eq. (14), we decomposed the spectral response of the N channel into the two different channels, the visible band and the NIR band. The N channel information in NIR band was recovered from the N channel that contained the energy of the entire spectrum of the image sensor. As a result, the decomposed N channel intensities in the NIR band and the RGB channel intensities in the NIR band were estimated from the result of Eq. (14). In Fig. 6, the relationship of the RGB channel intensities and the N channel intensity of 96 color patches of the Gretag color checker SG in the NIR band is represented. As described in the figure, they are asymptotically linear in the NIR band. From this correlation, the decomposed NIR band value of the RGB channel in the NIR band is defined as follows:

$$\begin{aligned}
 \hat{R}_{nir} &= \alpha_r \cdot \hat{N}_{nir} \\
 \hat{G}_{nir} &= \alpha_g \cdot \hat{N}_{nir} \\
 \hat{B}_{nir} &= \alpha_b \cdot \hat{N}_{nir}
 \end{aligned} \quad (15)$$

where  $\alpha_r$ ,  $\alpha_g$ , and  $\alpha_b$  represent the coefficients that show the linear correlation between the RGB channels and the N channel in the NIR band. From the equation, the intensities of the RGB channel in the NIR band were estimated and this color restoration model was processed with a single matrix transformation of:

$$(\hat{R}_{vis}, \hat{G}_{vis}, \hat{B}_{vis})^T = M \cdot (R, G, B, N)^T, \quad (16)$$

where  $M$  is

$$M = E + \frac{1}{K}AW, \quad (17)$$

where  $W$  is the N channel decomposition matrix,  $A$  is the RGB channel decomposition matrix, and  $E$  is a 3 by 4 matrix of zeros, with 1s along the leading diagonal. The N channel decomposition matrix  $W$  was defined as:

$$W = \begin{pmatrix} \omega_r & \omega_g & \omega_b & -1 \\ \omega_r & \omega_g & \omega_b & -1 \\ \omega_r & \omega_g & \omega_b & -1 \\ \omega_r & \omega_g & \omega_b & -1 \end{pmatrix}, \quad (18)$$

and the RGB channel decomposition matrix was defined as:

$$A = \begin{pmatrix} \alpha_r & 0 & 0 & 0 \\ 0 & \alpha_g & 0 & 0 \\ 0 & 0 & \alpha_b & 0 \end{pmatrix}. \quad (19)$$

Based on Eq. (17), the unified matrix  $M$  was:

$$M = \begin{pmatrix} \frac{\alpha_r \cdot \omega_r + K}{K} & \frac{\alpha_r \cdot \omega_g}{K} & \frac{\alpha_r \cdot \omega_b}{K} & -\frac{\alpha_r}{K} \\ \frac{\alpha_g \cdot \omega_r}{K} & \frac{\alpha_g \cdot \omega_g + K}{K} & \frac{\alpha_g \cdot \omega_b}{K} & -\frac{\alpha_g}{K} \\ \frac{\alpha_b \cdot \omega_r}{K} & \frac{\alpha_b \cdot \omega_g}{K} & \frac{\alpha_b \cdot \omega_b + K}{K} & -\frac{\alpha_b}{K} \end{pmatrix} \quad (20)$$

where  $K = \frac{\beta_{v,n} - 1}{\beta_{v,n}}$  is a scaling factor in Eq. (14),  $\omega_r(\lambda)$ ,  $\omega_g(\lambda)$ ,  $\omega_b(\lambda)$  are the coefficients for the linear combination in Eq. (9) and  $\alpha_r$ ,  $\alpha_g$ , and  $\alpha_b$  are the coefficients that represent the linear correlation between the RGB channels and the N channel in the NIR band in Eq. (15). The color restoration matrix restored the visible band intensity values from the observed cross-correlated RGBN values where the matrix coefficients were given by the visible band cross-correlation coefficients and the spectral cross-correlation coefficient.

## 4 EXPERIMENTAL RESULTS

We tested the method with several images captured under various lighting conditions: sunlight, incandescent lamp, and fluorescent lamp. For the training set for the correlation coefficients, we used the standard colors in the Macbeth SG color checkerboard.

In Figs. 8 (a) and (b), the visible band images observed by the MSFA sensor without and with the IRCF are depicted, respectively. In the figures, the effect of the NIR band energy on the color hue and saturation in all colors in color patches can be shown. Moreover, color degradation was highly distinctive in some materials such as fabrics since the NIR band energy had more effect on these materials. In Fig. 8(c), the result of the conventional method (G. D. Finlayson and Hubel, 2001) is described where the color saturation is far better than in Fig. 8(a). However,

Table 1: Average angular error.

	Average angular error ( $\times 10^{-2}$ )		
	Input image	Conventional method	Proposed method
Fluorescent	0.7651	0.7996	0.7716
Sunlight	6.9688	2.9261	1.5253
Incandescent	28.7329	7.7961	4.2263

the color saturation is still low with the high NIR reflectance materials, such as the yellow T-shirt and the black hat of the doll. In Fig. 8(d), the proposed method shows greater improvements than the conventional method with the vivid colors in the SG color chart and in the NIR sensitive materials. When compared with the visible band image in Fig. 8(b), the proposed method produces colors much more similar to the visible band color in both color patches and other materials.

In Fig. 7, the experimental results obtained under fluorescent lamp with 350lx illumination are depicted. Since the fluorescent lamp did not emit NIR band energy, the input image in Fig. 7 (a) and the optical filtered image in Fig. 7 (b) were almost the same. Because there was no distortion caused by the NIR band spectral energy in the input image, the proposed method in Fig. 7 (d) preserved the color of the input image. Figure 9 shows the experimental results in sunlight. Sunlight contains a wide range of spectral distribution and plenty of visible band information. In this case, we restored color with the proposed method in Eq. (20). When comparing figures 9 (c) to (d), the resulting image of the proposed method restored the distorted color well, especially the materials with high reflectance in the NIR band.

To demonstrate the similarity of the restored colors to the original visible band colors, the well known matric called angular error was used (K. Barnard and Funt, 2002). In this measurement, the color difference was calculated by the angle between the two color

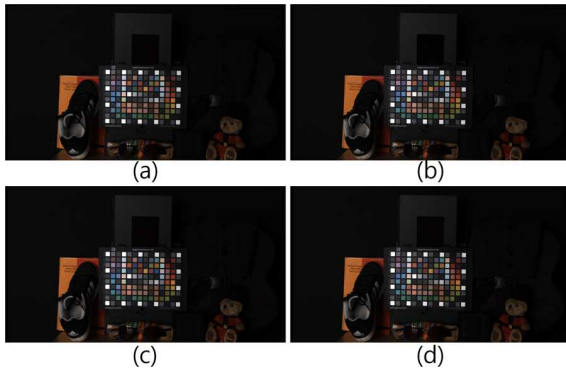


Figure 7: Experimental results under fluorescent lamp. (a) Input image. (b) Optical filtered visible band image. (c) LS based conventional method. (d) Proposed method.

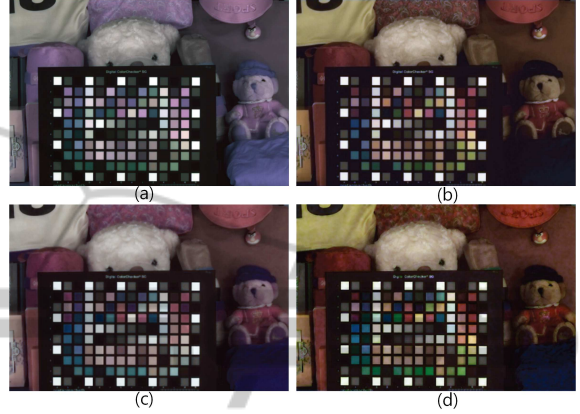


Figure 8: Experimental results under incandescent lamp. (a) Input image. (b) Optical filtered visible band image. (c) LS based conventional method. (d) Proposed method.

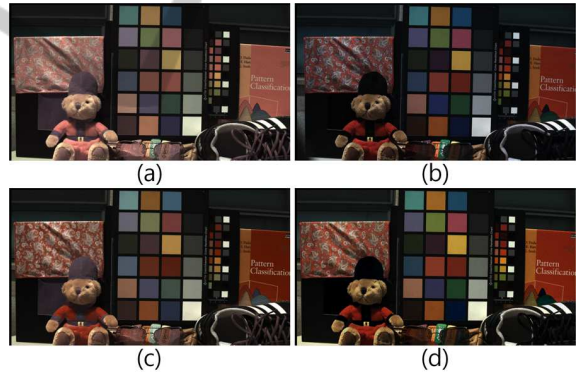


Figure 9: Experimental results under sunlight. (a) Input image. (b) Optical filtered visible band image. (c) LS based conventional method. (d) Proposed method.

vectors. In this estimation, the standard color patches and the colors in the fabric and in the leather were used as representatives.

In table 1, the average angular error of the standard color patches with a variety of light sources is described. The performance of the proposed method is well confirmed visually for materials with a large reflectance in the NIR band.

## 5 CONCLUSIONS

In this paper, a color restoration algorithm for an IRCF removed MSFA image sensor was proposed. For the spectrally degraded color information with RGB channels, the spectral estimation and spectral decomposition methods were used to the remove additional NIR band spectral information. Based on the filter correlation, the inter-channel correlations on the visible and NIR bands were assumed, respectively. When the N channel was decomposed into the visible and the NIR band information, the RGB channel in the visible band was finally restored with spectral decomposition. The experimental results show that the proposed method effectively restored the visible color from the color degraded images caused by IRCF removal.

## ACKNOWLEDGEMENTS

This work was supported by the National Research Foundation of Korea (NRF) grant funded by the Korea government (MSIP) (No. 2012R1A2A4A01003732).

## REFERENCES

- D. Yi, R. Liu, R. C. Z. L. and Li, S. Z. (2007). Face matching between near infrared and visible light images. In *Proc. IAPR/IEEE International Conference on Biometrics on*.
- Fredembach, C. and Susstrunk, S. (2008). Colouring the near-infrared. In *IS&T/SID 16th Color Imaging Conference*. SPIE.
- Fredembach, C. and Susstrunk, S. (2009). Illumination estimation and detection using near infrared. In *SPIE/IS&T Electronic Imaging, Digital Photography*. SPIE.
- G. D. Finlayson, S. D. H. (2000). Improving gamut mapping color constancy. *IEEE Transactions on Image Processing*, 9(10).
- G. D. Finlayson, S. D. H. and Hubel, P. M. (2001). Color by correlation: a simple, unifying framework for color constancy. *IEEE Transactions on Pattern Anal. and Machine Intell.*, 23(11).
- J. Choi, K. Y. and Kim, Y. (2011). A new adaptive component-substitution-based satellite image fusion by using partial replacement. *IEEE Transaction on Geoscience and Remote Sensing on*, 49(1).
- K. Barnard, V. C. and Funt, B. (2002). A comparison of computational color constancy algorithms - part i: methodology and experiments with synthesized data. *IEEE Transactions on Image Processing*, 11(9).
- Kumar, A. and Prathyusha, K. V. (2009). Personal authentication using hand vein triangulation and knuckle shape. *IEEE Transactions on Image Processing on*, 18(9).
- L. Schaul, C. F. and Susstrunk, S. (2009). Color image de-hazing using the near-infrared. In *IEEE International Conference on Image Processing*. IEEE.
- M. Kise, B. Park, G. W. H. K. C. L. and Windham, W. R. (2010). Multispectral imaging system with interchangeable filter design. *Computers and Electronics in Agriculture*, 72(2).
- Park, J. H. and Kang, M. G. (2004). Spatially adaptive multi-resolution multispectral image fusion. *International Journal of Remote Sensing on*, 25(23):5491–5508.
- S. Koyama, Y. Inaba, M. K. and Murata, T. (2008). A day and night visoin mos imager with robust pphotonic-crystal-based rgb-and-ir. *IEEE Transactions on Electron Devices*, 55(3).
- S. Matsui, T. Okabe, M. S. and Sato, Y. (2010). Image enhancement of low-light scenes with near-infrared flash images. In *Lecture Notes in computer Science: Computer Vision*. SPIE.
- S. Z. Li, C. RuFeng Chu, L. S. and Lun, Z. (2007). Illumination invariant face recognition using near-infrared images. *IEEE Transactions on Pattern Analysis and Machine Intelligence on*, 29(4).
- Salamati, N. and Susstrunk, S. (2010). Material-based object segmentation using nir information. In *IS& T/SID 18th Color Imaging Conference on*. SPIE.
- X. Hao, H. Chen, C. Y. N. Y. H. B. and Wang, C. (2010). A near-infrared imaging method for capturing the interior of a vehicle through windshield. In *2010 IEEE Southwest Symposium on Image Analysis & Interpretation on*. IEEE.